Research Article | Open Access

Greenverse Science

Bi *et al. Greenverse Sci.* **2026**, *1*, 11 **DOI:**10.20517/greenvsci.2026.10

Acid-modified Pd-UiO-67 for o-xylene degradation: residual Cl species removal and regulation of Cl-containing byproducts formation

Fukun Bi[1], Haiyang Yu[1], Jiale Ma[1], Jianghua Huang[1], Heming Wang[1], Jiafeng Wei[1], Quanxin Du[1], Yuandong Huang[1], Xiaodong Zhang[1,2,3,*]

Keywords:
Pd-UiO-67 catalysts, catalytic oxidation, VOCs, residual Cl, Cl-containing byproducts

Citation: Bi, F.; Yu, H.; Ma, J.; Huang, J.; Wang, H.; Wei, J.; Du, Q.; Huang, Y.; Zhang, X. Acid-modified Pd-UiO-67 for o-xylene degradation: residual Cl species removal and regulation of Cl-containing byproducts formation. *Greenverse Sci.* **2026**, *1*, 11. https://dx.doi.org/10.20517/greenvsci.2026.10

Received: 22 Apr 2026
First Decision: 21 May 2026
Revised: 26 May 2026
Accepted: 4 Jun 2026
Published: 24 Jun 2026

Academic Editor: Dengsong Zhang
Copy Editor: Xing-Yue Zhang
Production Editor: Xing-Yue Zhang

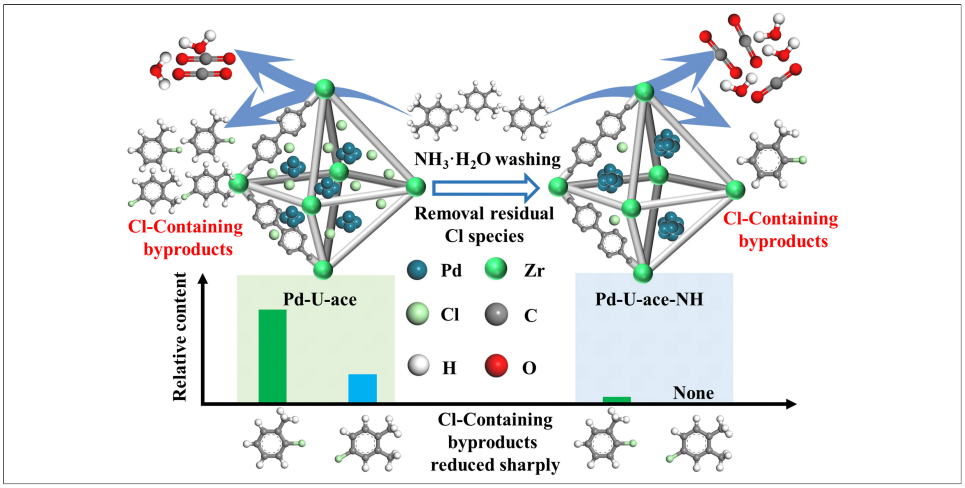

Abstract

Metal-organic frameworks (MOFs), particularly Zr-based UiO series, have emerged as promising supports for noble metals owing to their high porosity and tunable structures. However, residual Cl species originating from metal precursors, such as $ZrCl_4$, in MOF-based catalysts are frequently overlooked, which can participate in volatile organic compounds (VOCs) degradation and generate toxic Cl-containing byproducts. Herein, acetic acid-modified UiO-67 (U-ace) was used as the support, and two effective strategies, including silver nitrate precipitation and dilute ammonia washing, were adopted to remove residual Cl species, fabricating a series of supported Pd catalysts for o-xylene catalytic oxidation. The physicochemical properties of the as-prepared catalysts were systematically characterized, and their catalytic activity and chlorinated byproduct distribution were comprehensively investigated. The results showed that both Cl removal methods effectively reduced the residual Cl species, and dilute ammonia washing achieved the lowest residual Cl content (0.08 wt%). However, Cl removal induced a decrease in surface Pd^0 species, promoted Pd nanoparticle aggregation, and reduction of linker defects, resulting in a slight decline in catalytic activity. Importantly, thermal desorption-gas

[1]School of Environment and Architecture, University of Shanghai for Science and Technology, Shanghai 200093, China.
[2]State Key Laboratory of Plateau Ecology and Agriculture, Qinghai University, Xining 810016, Qinghai, China.
[3]Shanghai Non-carbon Energy Conversion and Utilization Institute, Shanghai 200240, China.

[*]**Correspondence to:** Prof. Xiaodong Zhang, School of Environment and Architecture, University of Shanghai for Science and Technology, Shanghai 200093, China. E-mail: zhangxiaodong@usst.edu.cn

chromatograph-mass spectrometer analysis confirmed that Cl removal significantly suppressed the formation of typical chlorinated byproducts (2-chlorotoluene and 4-chloro-1,2-dimethylbenzene); particularly, Pd-U-ace-NH almost eliminated 4-chloro-1,2-dimethylbenzene and only produced trace 2-chlorotoluene. Furthermore, Pd-U-ace-NH exhibited excellent long-term stability, water resistance, and recyclability. This work presents an economical and efficient strategy for residual Cl removal in MOF-based catalysts, offering guidance for designing environmentally friendly catalysts for practical VOC elimination.

INTRODUCTION

Volatile organic compounds (VOCs), as the typical air pollutants emitted from petrochemical, coating, and industrial combustion processes, are key precursors of ozone (O_3) and fine particulate matter ($PM_{2.5}$), and aromatic VOCs such as o-xylene also pose significant carcinogenic risks to human health[1,2]. Consequently, the development of effective VOC abatement technologies is of paramount urgency. In recent years, numerous technologies have been developed to reduce VOC emissions, including absorption[3], adsorption[4,5], photocatalysis[6,7], photothermal catalysis[8-10], and catalytic oxidation[11-14], *etc.*, have been developed. Among the various technologies, catalytic oxidation is recognized as the most promising VOC elimination technology owing to its high efficiency, low energy consumption, and minimal secondary pollution, and the core of this technology lies in the development of high-performance catalysts[15,16]. Supported noble metal catalysts, particularly supported Pd catalysts, have attracted extensive attention due to their outstanding low-temperature activity and oxygen activation ability. Meanwhile, metal-organic frameworks (MOFs) with high specific surface areas, tunable pore structure, and excellent thermal stability represent ideal supports for dispersing noble metal nanoparticles[17-19].

Zr-based UiO series MOFs, especially UiO-66 and UiO-67, have become a major research focus in VOC catalytic degradation owing to their exceptional structural stability and defect engineering tunability[20]. Acid modification can introduce abundant linker defects into UiO-67, which not only enhances the adsorption capacity of VOC molecules but also provides anchoring sites for noble metal species, thereby improving the dispersion of active metals and catalytic performance[21,22]. For example, Su *et al.*[23] prepared defective UiO-67 by using benzoic acid as the modulator. The open-pore structure of the defective framework facilitates substrate adsorption, while the confinement effect of the framework inhibits the aggregation of Pd, ensuring the good dispersion of Pd species, and enhancing the catalytic performance. Meanwhile, our previous work[24] also confirmed that an acid-modified UiO-67 supported Pd catalyst exhibited improved o-xylene catalytic degradation, which was attributed to defective sites in UiO-67 confining the growth of Pd species, and promoting its high dispersion. However, $ZrCl_4$, the most commonly used metal precursor for Zr-UiOs synthesis, inevitably introduces residual Cl species into the framework. Our previous work[25] demonstrated that these residual Cl species can participate in the electrophilic substitution reactions of aromatic VOCs during degradation, generating a variety of toxic chlorinated byproducts, even dioxin precursors such as dichlorobenzene, which pose new environmental risk yet remain widely neglected in current research. Although we have conducted preliminary investigations into the methods for removing residual Cl species from MOF materials, such as precursor substitution and post-treatment, there are still significant limitations. Furthermore, the regulation mechanism of Cl removal on the microstructure, Pd valence state, catalytic activity, and byproduct distribution of acid-modified UiO-67 remains unclear. Therefore, it is urgent to develop an economical and efficient Cl removal strategy compatible with practical application conditions.

Herein, acetic acid-modified UiO-67 was selected as the support, and silver nitrate precipitation (with-/without filtration) and dilute ammonia washing were employed to remove residual chlorine species for the preparation of supported Pd catalysts. The effects of different Cl removal methods on the crystal structure, pore properties, surface chemical state, Pd dispersion, and defect content of the catalysts were systematically characterized. The catalytic degradation performance of o-xylene and the distribution of Cl-containing byproducts were investigated. Additionally, the stability, water resistance, and

recyclability of the optimal catalyst were evaluated. This work aims to solve the key problem of toxic byproduct generation caused by residual Cl in MOF catalysts, and provides technical support and theoretical basis for the green industrial application of UiO-series catalysts in VOC purification.

EXPERIMENTAL

Materials and chemicals

Zirconium tetrachloride ($ZrCl_4$, 98%) and palladium acetate ($Pd(OAc)_2$, Pd > 47.4%) were purchased from Aladdin. 4,4'-Biphenyldicarboxylic acid (BPDC, 98%+) was purchased from Adamas. N,N-dimethylformamide (DMF, 99.5%), glacial acetic acid (99.5%), silver nitrate ($AgNO_3$, 99.8%), ammonium hydroxide ($NH_3 \cdot H_2O$, 25%~28%), and ethanol (99%) were obtained from Sinopharm Chemical Reagent Co., Ltd. All chemicals were used as received without further purification.

Synthesis of the different UiO-67 supports

The acetic acid-modified UiO-67, denoted U-ace, was synthesized as described in our previous work[24] using acetic acid as the modulator. The detailed synthesis procedure is provided in Supplementary Text 1. Cl-removed UiO-67 supports were prepared via the silver nitrate precipitation method and the dilute ammonia water washing method as reported in our previous work[25]. For the silver nitrate precipitation method, the synthesis process was similar to the preparation of U-ace, except that excess $AgNO_3$ (molar ratio of $ZrCl_4$ to $AgNO_3$ is 1:4.2) was added and sonicated for 30 min prior to transferring the mixture into the Teflon reactor. After the addition of $AgNO_3$ into the mixed solution, a white AgCl precipitate was observed. During this process, when the AgCl precipitate is not filtered out during the hydrothermal crystallization process, U-ace-SN can be obtained. Conversely, if AgCl was filtered out before hydrothermal crystallization, U-ace-SN-F can be obtained. For the dilute ammonia water washing method, 1.0 g of as-prepared U-ace was washed with 150 mL of dilute aqueous ammonia (pH = 9~10) for 24 h under magnetic stirring. The resulting white powder, denoted U-ace-NH, was collected by centrifugation, washing with deionized water for 3 times, and drying at 70 °C overnight.

Synthesis of the supported Pd catalysts

The supported Pd catalysts were prepared via the wet-impregnation method as described in our previous work[26]. The detailed synthesis procedure is provided in Supplementary Text 2. The supported Pd catalysts with the theoretical Pd loading of 1.0 wt% were synthesized by using U-ace, U-ace-SN, U-ace-SN-F, and U-ace-NH as the supports, and were denoted Pd-U-ace, Pd-U-ace-SN, Pd-U-ace-SN-F, and Pd-U-ace-NH, respectively. The actual Pd loadings of the supported Pd catalysts, determined by inductively coupled plasma optical emission spectrometer (ICP-OES) were 1.46, 1.41, 1.48, and 1.44 wt% for Pd-U-ace, Pd-U-ace-SN, Pd-U-ace-SN-F, and Pd-U-ace-NH, respectively. The physicochemical properties of the as-prepared supported Pd catalysts were systematically characterized using various techniques. For the detailed information, please refer to Supplementary Text 3.

Catalytic performance test

The catalytic performance of the as-prepared samples was evaluated in a custom-built fixed-bed reactor using o-xylene as the model molecule. 0.1 g of the catalyst with the particle size of 20-40 mesh was placed in a U-typed quartz tube. Then, the reaction gases, 1,000 ppm o-xylene and 20.0 vol.% O_2, balanced with Ar, were introduced to the reaction system. The total gas flow rate was maintained at 50 mL/min, namely, the weight hourly space velocity (WHSV) was 30,000 mL/(g·h). The reaction temperature was controlled by a temperature controller. The inlet and outlet o-xylene and CO_2 concentrations were analyzed by an online gas chromatograph (GC, GC2060, Ruimin, Shanghai) equipped with two flame ionization detectors (FIDs). At each temperature, the o-xylene and CO_2 concentrations were determined three times to calculate the average concentration, and the average o-xylene and CO_2 concentrations were used to calculate o-xylene conversion and CO_2 yield. The detailed calculation, kinetic study, and water resistance test could be found in Supplementary Text 4.

RESULTS AND DISCUSSION

Characterization of the supported Pd catalysts

The crystal structures of the supported Pd catalysts were characterized via X-ray diffraction (XRD). As shown in Figure 1A, all the supported Pd catalysts present the characteristic XRD diffraction peaks of UiO-67[24]. Meanwhile, compared with Pd-U-ace, the characteristic diffraction peaks of UiO-67 are

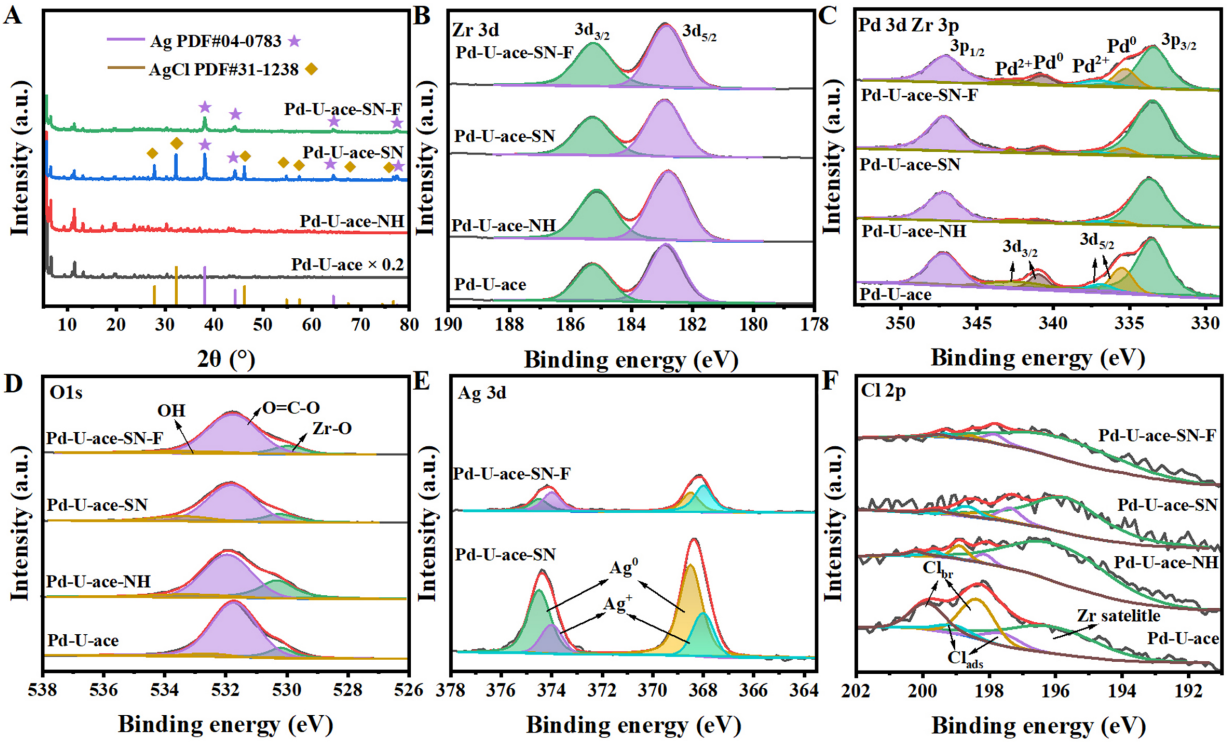

Figure 1. XRD patterns (A), and Zr 3d (B), Pd 3d Zr 3p (C), O 1s (D), Ag 3d (E), and Cl 2p (F) XPS spectra of Pd-U-ace[24], Pd-U-ace-NH, Pd-U-ace-SN, and Pd-U-ace-SN-F. XRD: X-ray diffraction; XPS: X-ray photoelectron spectroscopy; PDF: Powder Diffraction File.

retained but their intensities are weakened in the treated samples, indicating that the UiO-67-supported Pd catalysts with slightly reduced crystallinity were successfully synthesized[27]. The successful synthesis of the UiO-67 supports and their corresponding Pd catalysts was further confirmed by the Fourier transform infrared (FT-IR) spectra [Supplementary Figure 1]. Notably, no diffraction peaks corresponding to Pd species were detected in the XRD patterns, which can be attributed to the low Pd loading and/or high dispersion of Pd nanoparticles[28,29]. Importantly, the typical diffraction peaks of metallic Ag and AgCl could be found in Pd-U-ace-SN, while only Ag could be observed in Pd-U-ace-SN-F, which suggested the bulk AgCl was removed by filtration. The addition of excess $AgNO_3$ led to the formation of residual Ag particles in the samples. Furthermore, the presence of residual Ag particles in Pd-U-ace-SN and Pd-U-ace-SN-F was further confirmed by the UV-vis diffuse reflectance spectra (UV-vis DRS) [Supplementary Figure 2]. The surface area and pore structure of the as-prepared samples were characterized by physical absorption. All the samples exhibit typical type I adsorption isotherms [Supplementary Figure 3A], suggesting that the catalysts were micropore materials. Notably, compared with Pd-U-ace, the micropore volumes of Pd-U-ace-NH, Pd-U-ace-SN, and Pd-U-ace-SN-F decreased, while mesopores were formed [Supplementary Figure 3B and C], indicating that the dilute ammonia washing and silver nitrate precipitation methods induced the slight destruction of the micropore structure of UiO-67. Concurrently, these pretreatment methods resulted in an increase in total pore volume and a decrease in surface area [Supplementary Figure 3D and Supplementary Table 1].

The surface chemical composition and state of the catalysts were characterized by X-ray photoelectron spectroscopy (XPS). As presented in Figure 1B, the Zr 3d orbital exhibits two characteristic peaks at 182.9 and 185.3 eV, corresponding to the Zr $3d_{5/2}$ and Zr $3d_{3/2}$, respectively[30]. The Pd species [Figure 1C] could be found in 335.5, 337.0, 341.0, and 342.6 eV, corresponding to the Pd^0 and Pd^{2+} species in $3d_{5/2}$ and $3d_{3/2}$ orbits, respectively[25,31]. Meanwhile, the molar ratios of $Pd^0/(Pd^0 + Pd^{2+})$ calculated from the XPS spectra are summarized in Supplementary Table 1. Pd-U-ace possesses the largest $Pd^0/(Pd^0 + Pd^{2+})$ value (0.76), followed by Pd-U-ace-SN-F (0.73), Pd-U-ace-SN (0.68) and Pd-U-ace-NH

(0.52). The O 1s spectra [Figure 1D] were divided into Zr-O and O=C-O in the UiO-67 framework, and the surface adsorbed OH species[32]. Ag species in Pd-U-ace-SN and Pd-U-ace-SN-F are illustrated in Figure 1E. Ag^+ and Ag^0 species can be observed in Pd-U-ace-SN and Pd-U-ace-SN-F[33]. Compared with Pd-U-ace-SN, the peak intensity of Ag 3d in Pd-U-ace-SN-F decreased greatly, suggesting that the AgCl and some Ag species were removed via filtration, which is consistent with the XRD results. The Cl 2p orbits of the supported Pd catalysts are displayed in Figure 1F. Compared with Pd-U-ace, the surface adsorbed Cl (Cl_{ads}) species (197.6 and 199.9 eV) and bridged Cl (Cl_{br}) species (198.4 and 199.9 eV) in Pd-U-ace-NH, Pd-U-ace-SN, and Pd-U-ace-SN-F reduced greatly, confirming that dilute ammonia washing and silver nitrate precipitation methods could effectively remove residual Cl species in the framework of UiO-67[34-36].

The morphology and Pd distribution of the supported Pd catalysts were investigated by the transmission electron microscope (TEM) and high-resolution TEM (HRTEM). As shown in Figure 2A, Pd-U-ace-NH retains the typical octahedral morphology, suggesting that the framework of UiO-67 was not destroyed after dilute ammonia water treatment. Meanwhile, Pd particles with a lattice spacing of 0.22 nm corresponding to the (111) crystal facet were observed [Figure 2Aii-iv]. Compared with Pd-U-ace with the average Pd particle size of 3.7 nm[24], after the treatment of UiO-67 support by dilute ammonia water, the average Pd particle size was increased to 6.10 nm [Supplementary Figure 4]. Additionally, C, O, Zr, and Pd were uniformly distributed in Pd-U-ace-NH [Figure 2Av-vii]. The residual Cl species was reduced from 0.28 wt% in Pd-U-ace[24] to 0.08 wt% in Pd-U-ace-NH. Figure 2B and C present the TEM, HRTEM, and corresponding elements mapping of Pd-U-ace-SN and Pd-U-ace-SN-F, respectively. Some large particles (red circle) can be found in Pd-U-ace-SN [Figure 2Bi and ii]. The (111) crystal facet of Pd, Ag, and AgCl is also observed in the HRTEM of Pd-U-ace-SN [Figure 2Biii and iv], which indicates that the large AgCl and Ag particles were formed in Pd-U-ace-SN. This was consistent with XRD results. Additionally, the aggregated Pd species was also found [Figure 2Bv-vii], suggesting that the presence of Ag species might induce the aggregation of Pd particles. The presence of residual Cl species in Pd-U-ace-SN-F was determined to 0.16 wt%. After the filtration of AgCl during the silver nitrate precipitation process, the bulk particles in Pd-U-ace-SN-F [Figure 2Ci and ii] were reduced greatly, which suggested that most of the large particles in Pd-U-ace-SN were AgCl. Similarly, the (111) crystal face of Pd, Ag, and AgCl was determined in Pd-U-ace-SN-F [Figure 2Ciii and iv], suggesting that the filtration cannot remove AgCl thoroughly. Meanwhile, the aggregation of Pd was also observed, and the residual Cl species was determined to 0.16 wt% [Figure 2Cv-vii]. According to the above analysis, it could be found that after the removal of residual Cl species, the Pd particle size in the supported Pd catalysts became larger. Especially, after the treatment by silver nitrate precipitation, the Pd particles were aggregated obviously, and the presence of bulk AgCl and Ag particles was observed. The residual Cl species in Pd-U-ace-NH, Pd-U-ace-SN, and Pd-U-ace-SN-F were measured as 0.08, 0.21, and 0.16 wt%, respectively, confirming that dilute ammonia water washing is an economical and effective method for removing residual Cl species.

To investigate the effect of dilute ammonia water treatment and silver nitrate precipitation on the defect structures of the catalysts, thermogravimetry (TG) and ^{1}H nuclear magnetic resonance (^{1}H NMR) were performed. Figure 3A-D presents the TG and DTG curves of the supported Pd catalysts. The TG curves exhibit three distinct weight loss stages at the temperature of < 100 °C, 100-350 °C and 350-550 °C, which were attributed to the volatilization of the H_2O and organic solvent residual in the pore channels, the decomposition of the unstable organic carboxylic acid ligands and the thermal decomposition of the UiO-67 framework, respectively. The complete collapse temperatures were 550, 500, 510, and 450 °C for Pd-U-ace, Pd-U-ace-NH, Pd-U-ace-SN, and Pd-U-ace-SN-F, respectively. This indicates that the thermal stability of the materials decreased following residual Cl removal via dilute ammonia washing or silver nitrate precipitation, with Pd-U-ace-SN-F showing the most significant stability loss. The weightlessness ratios of Pd-U-ace, Pd-U-ace-NH, Pd-U-ace-SN and Pd-U-ace-SN-F were determined to be 52.83%, 49.89%, 28.86% and 51.83%, respectively. Theoret-

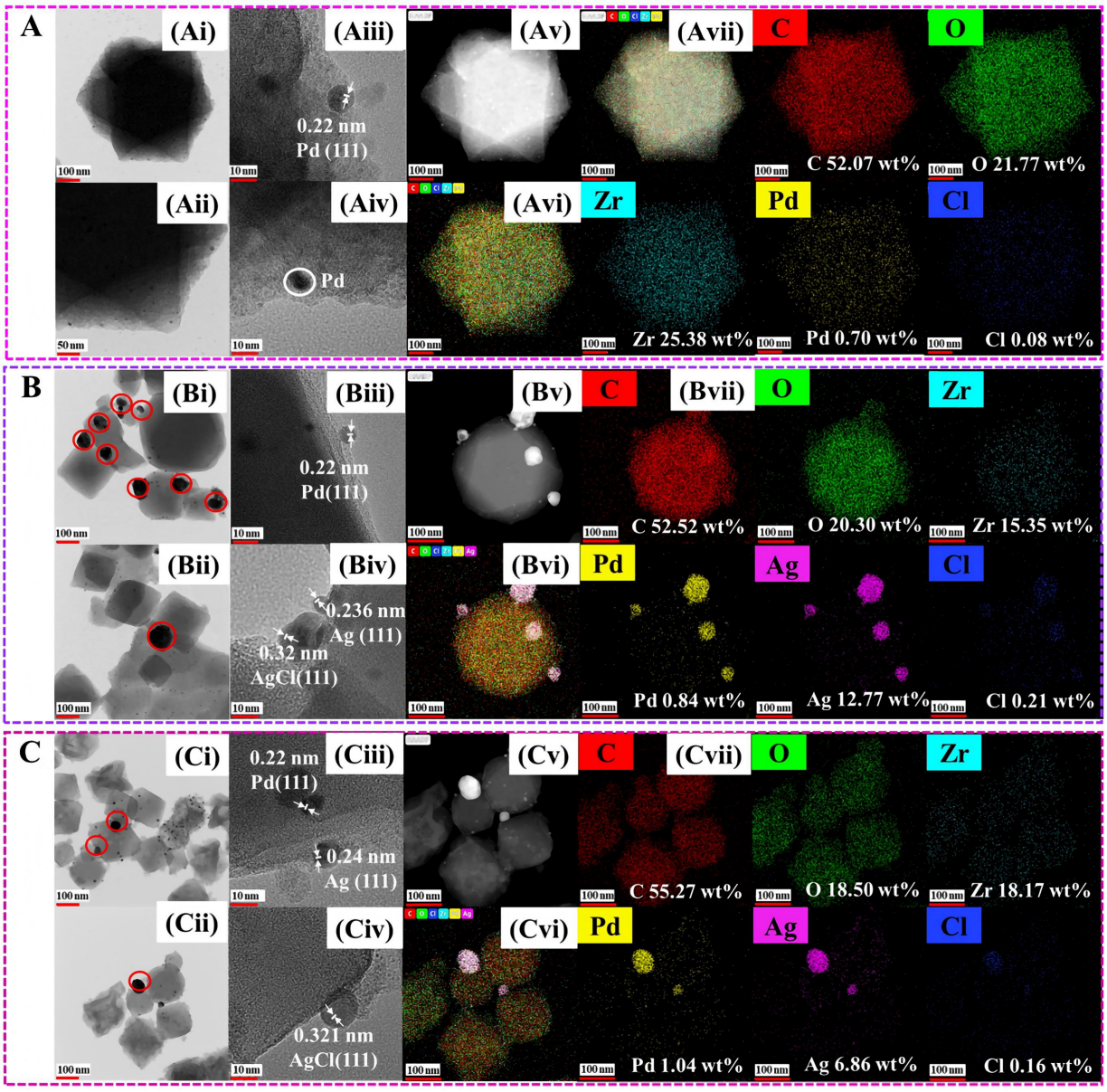

Figure 2. TEM (i, ii), HRTEM (iii, iv), HAADF (v) images and the corresponding elements mapping (vi, vii) of Pd-U-ace-NH (A), Pd-U-ace-SN (B) and Pd-U-ace-SN-F (C). TEM: Transmission electron microscope; HRTEM: high-resolution TEM; HAADF: high-angle annular dark-field.

ically, the weightlessness ratio of UiO-67 with the framework of $Zr_6O_6(BPDC)_6$ is 64.5%, which is higher than that of these supported Pd catalysts. This suggested the presence of defects in the as-prepared Pd catalysts. Notably, Pd-U-ace-SN possesses the lowest weightlessness ratio, which was attributed to the presence of a large amount of AgCl in the sample. To further investigate the number of link defects, a $_1$H NMR was performed. As shown in Figures 3E and 3F, the calculated numbers of missing links were 3.24, 2.89, 3.88, and 2.67 for Pd-U-ace, Pd-U-ace-NH, Pd-U-ace-SN, and Pd-U-ace-SN-F, respectively. Although the number of missing chains of Pd-U-ace-SN was the highest, due to the presence of a large amount of AgCl precipitation in its structure, the amount of UiO-67 in this catalyst was relatively small. Therefore, the actual number of missing links will be much lower than 3.88. According to the above, after the residual Cl species removal, the number of defects in the catalyst would decrease as follows: Pd-U-ace > Pd-U-ace-SN-F > Pd-U-ace-SN > Pd-U-ace-NH.

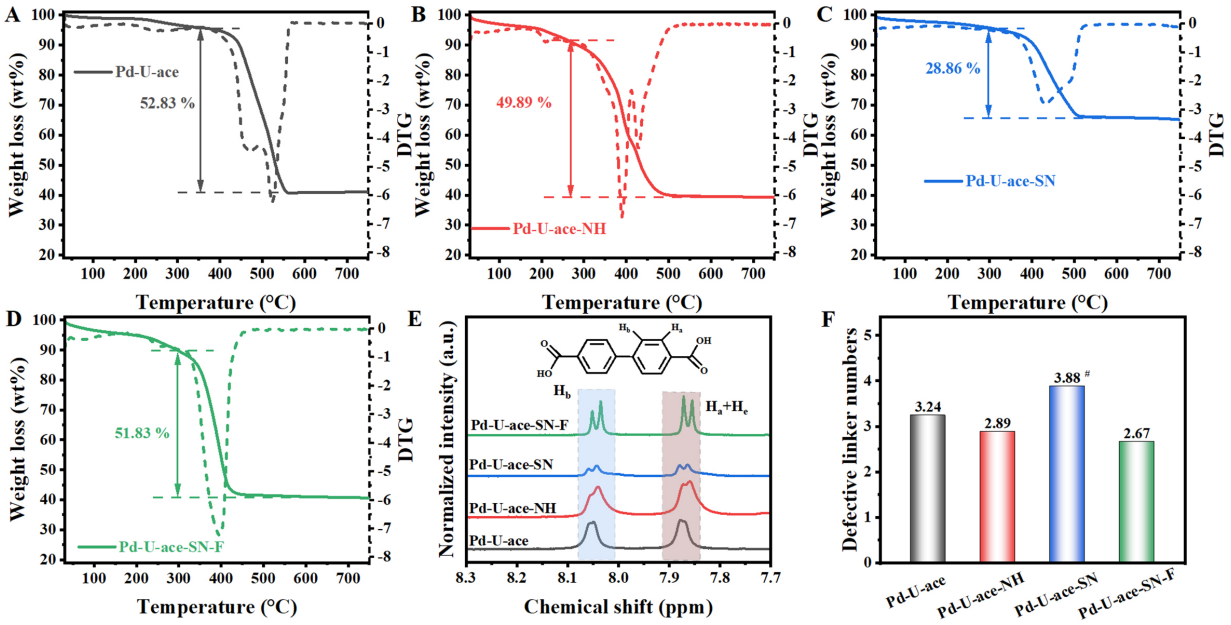

Figure 3. TG and DTG curves of Pd-U-ace[24] (A), Pd-U-ace-NH (B), Pd-U-ace-SN (C), and Pd-U-ace-SN-F (D); ^{1}H NMR patterns (E) and corresponding defective linker numbers (F) of Pd-U-ace[24], Pd-U-ace-NH, Pd-U-ace-SN, and Pd-U-ace-SN-F (#The apparent defect value of Pd-U-ace-SN cannot be directly compared with others due to the AgCl impurity phase.). TG: Thermogravimetry; DTG: derivative thermogravimetry.

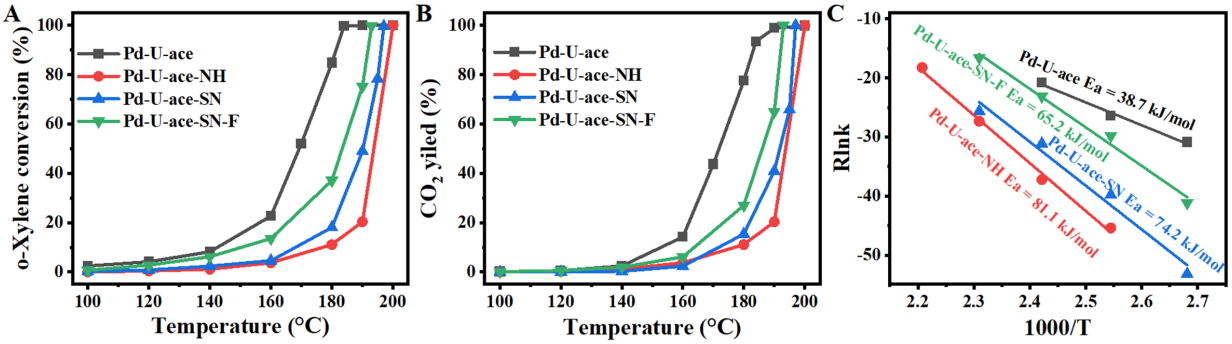

Figure 4. Catalytic performance of Pd-U-ace[24], Pd-U-ace-NH, Pd-U-ace-SN, and Pd-U-ace-SN-F for o-xylene degradation: (A) o-xylene conversion and (B) CO_2 yield, and (C) the corresponding Ea plots.

Catalytic performance of the supported Pd catalysts

The catalytic performance of the as-prepared catalysts was evaluated for o-xylene catalytic degradation [Figure 4]. Meanwhile, the temperatures at which o-xylene conversion reached 10%, 50%, and 90% (T_{10}, T_{50}, and T_{90}) were also calculated [Supplementary Table 2]. As displayed in Figure 4A and Supplementary Table 2, Pd-U-ace exhibits the optimal o-xylene degradation performance with the lowest T_{90} value of 181 °C, followed by Pd-U-ace-SN-F (192 °C), Pd-U-ace-SN (196 °C) and Pd-U-ace-NH. The curves of CO_2 yield present a similar tendency to that of o-xylene conversion. However, at any given temperature, the CO_2 yield is significantly lower than the o-xylene conversion [Figure 4B], indicating the generation of intermediates during o-xylene degradation. To further assess the intrinsic catalytic activity of the supported Pd catalysts, the reaction activation energy (Ea) was calculated using the Arrhenius equation based on the o-xylene conversion below 20% [Figure 4C and Supplementary Table 2]. The lowest Ea value of 38.7 kJ/mol for Pd-U-ace also confirmed its optimal catalytic activity. It is well established that the catalytic activity of a catalyst is closely related to its physicochemical prop-

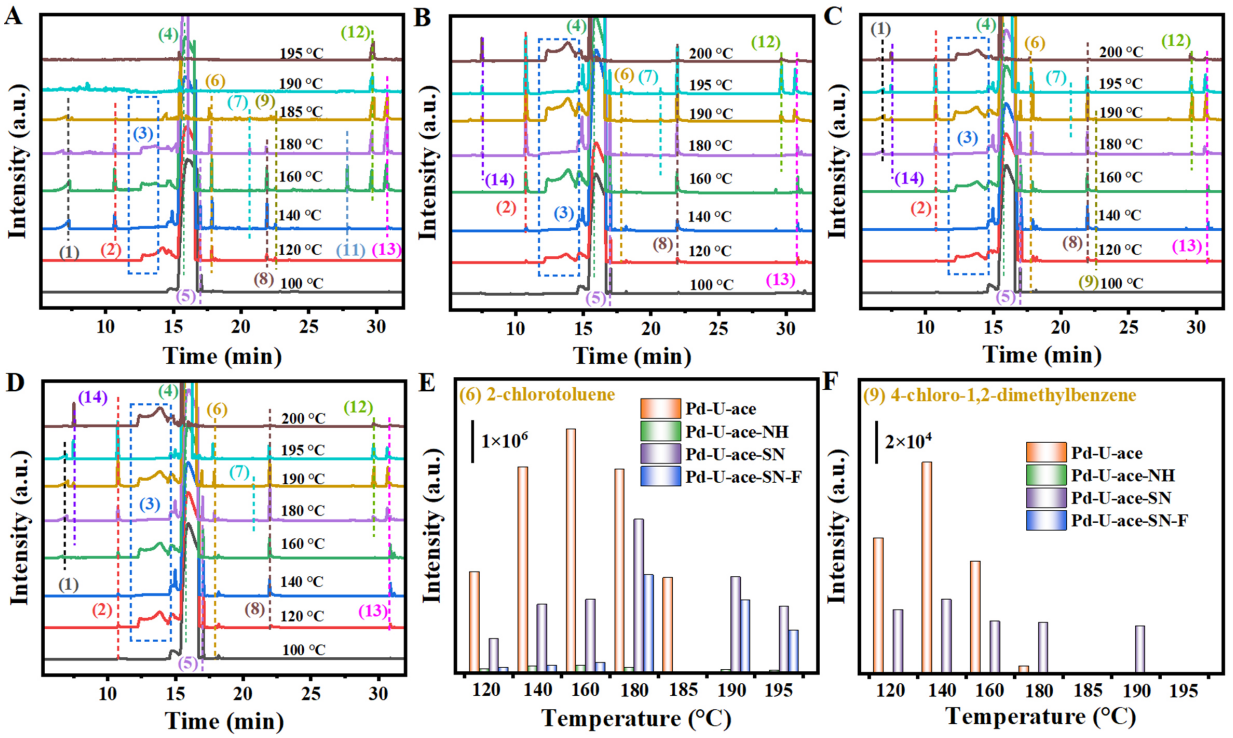

Figure 5. TD-GC-MS total ion current chromatograms of Pd-U-ace[24] (A), Pd-U-ace-NH (B), Pd-U-ace-SN (C), and Pd-U-ace-SN-F (D) for o-xylene degradation; the distributions of (6) 2-chlorotoluene (E) and (9) 4-chloro-1,2-dimethylbenzene (F) generated over the supported Pd catalysts (The corresponding products of serial numbers are summarized in Supplementary Table 3). TD-GC-MS: Thermal desorption-gas chromatograph-mass spectrometer.

erties[37,38]. According to the characterization results, it could be found that after the removal of residual Cl species, the surface Pd^0 species in the supported Pd catalysts was decreased [Figure 1C and Supplementary Table 1] and the Pd particles exhibited varying degrees of aggregation [Figure 2]. Furthermore, the defects in the supported Pd catalysts were reduced [Figure 3]. Based on the above factors, the catalytic performance of the supported Pd catalysts that removed residual Cl species via dilute ammonia solution washing and silver nitrate precipitation methods was significantly declined.

o-Xylene degradation intermediates and distribution of Cl-containing byproducts

In our previous work[25], we found that the presence of residual Cl species in Zr-MOFs supported Pd catalysts would participate in VOCs degradation, leading to the formation of Cl-containing byproducts. Therefore, to investigate the o-xylene degradation intermediates, especially Cl-containing byproducts, generated over the various supported Pd catalysts and the removal efficiency of residual Cl species, the thermal desorption-gas chromatograph-mass spectrometer (TD-GC-MS) was performed at different temperatures. Figure 5A-D illustrates the TD-GC-MS chromatograms of the various supported Pd catalysts for o-xylene degradation, and the corresponding intermediates of the serial numbers are summarized in Supplementary Table 3. The generation of o-xylene degradation intermediates [Figure 5A] and the possible o-xylene degradation pathway had been analyzed and discussed in detail in our previous work[24]. Herein, the o-xylene degradation intermediates generated over the residual Cl removed catalysts were focused on.

As shown in Figure 5A-D and Supplementary Table 3, compared with Pd-U-ace, most of the degradation intermediate products of o-xylene can be detected in the Pd-U-ace-NH, Pd-U-ace-SN, and Pd-U-ace-SN-F, except for (11) 2-methylbenzyl acetate. Meanwhile, the acetic acid, which might originate from the regulator, decreased greatly in the Pd-U-ace-SN and Pd-U-ace-SN-F, and even disappeared in Pd-U-ace-NH. Generally, the addition of an acid modulator would compete with organic linkers for coordination with metal clusters, inducing

the formation of missing-linker defects in the MOF framework[39]. Therefore, it could be inferred that the addition of $AgNO_3$ during the preparation of acetic acid-modified UiO-67 would influence the competition between acetic acid and organic linkers, causing a decrease in the formation of missing linker defects and the residual acetic acid. Furthermore, the decrease of acetate acid suppressed the generation of (11) 2-methylbenzyl acetate. Notably, compared with Pd-U-ace, (14) benzene was detected over Pd-U-ace, Pd-U-ace-SN, and Pd-U-ace-SN-F, which might be ascribed to the decrease in catalytic activity of these catalysts, reducing the further oxidation of benzene.

Notably, although the residual Cl species can be effectively removed through dilute ammonia water washing and silver nitrate precipitation, Cl-containing byproducts (6) 2-chlorotoluene and (9) 4-chloro-1,2-dimethylbenzene still exist after chlorine removal. To further analyze the generation of Cl-containing byproducts and their distribution, the peak areas of the corresponding TD-GC-MS patterns were integrated [Figures 5E and F]. As shown in Figures 5E and F, compared with Pd-U-ace, the generation of (6) 2-chlorotoluene and (9) 4-chloro-1,2-dimethylbenzene greatly decreased or even disappeared over Pd-U-ace-NH, Pd-U-ace-SN, and Pd-U-ace-SN-F, which suggested the effectiveness of these dechlorination methods. In particular, only a trace amount of (6) 2-chlorotoluene was detected over the catalyst prepared via the dilute ammonia solution washing treatment. No (9) 4-chloro-1,2-dimethylbenzene was detected. These results demonstrated the effectiveness of the dilute ammonia water washing method for Cl removal. The detection of a large amount of (6) 2-chlorotoluene and (9) 4-chloro-1,2-dimethylbenzene over Pd-U-ace-SN might be related to the presence of residual AgCl. According to the above, it could be concluded that the catalyst obtained through the ammonia water washing method for residual Cl removal has a better inhibitory effect on the formation of Cl-containing by-products in comparison to the silver nitrate precipitation method. It effectively controls the generation of intermediate chlorine-containing by-products. Since ammonia water is more economical and silver nitrate is more expensive, in practical applications, the ammonia water washing method can be adopted to remove the chlorine element from the catalyst, preparing a more environmentally friendly catalyst, and achieving the purpose of eliminating by-products during the catalytic degradation of VOCs.

As mentioned above, the Pd-U-ace-NH catalyst prepared using U-ace-NH that has been treated with dilute ammonia water can effectively prevent the formation of Cl-containing byproducts during the catalytic degradation of o-xylene. In practical applications, the stability, reusability, and water resistance of the catalyst are also crucial factors in evaluating the performance of the catalyst. As shown in Supplementary Figure 5, Pd-U-ace-NH presents great long-term stability for o-xylene degradation. Although the competitive adsorption of water vapor and o-xylene in humid conditions would lead to a decrease in the catalytic activity of o-xylene [Supplementary Figure 6A], the o-xylene conversion would rapidly recover after the water vapor was shut off [Supplementary Figure 6B], indicating that Pd-U-ace-NH has good water resistance. Our previous work[24] found that the introduction of H_2O during o-xylene oxidation over Pd-U-ace promoted the formation of more Cl-containing byproducts. Therefore, to investigate the influence of H_2O on Cl-containing byproducts formation over Pd-U-ace-NH, the TD-GC-MS spectra were collected during o-xylene oxidation in the presence of 5.0 vol.% H_2O over Pd-U-ace-NH. As presented in Supplementary Figure 7, compared with the dry condition [Figure 5B and Supplementary Table 3], no more Cl-containing byproducts were detected after introducing water vapor, which further indicates the high efficiency of the dilute ammonia water washing method for residual Cl removal. Additionally, the cycle test [Supplementary Figure 8] suggested that Pd-U-ace-NH presented great reusability. Furthermore, after being reused several times, the catalytic performance of the Pd-U-ace-NH was improved. Characterization results of the Pd-U-ace-NH after o-xylene degradation reaction (Pd-U-ace-NH-A) indicated that after the reaction, the functional group structure was retained [Supplementary Figure 9A], indicating the o-xylene degradation reaction did not destroy the structure of Pd-U-ace-NH. The surface area and total pore volume [Supplementary Figure 9B-D and Supplementary Table 4] of Pd-U-ace-NH-A were increased. Meanwhile, the TEM and HRTEM results [Supplementary Figure

10] showed that the octahedral structure and Pd particles were maintained in Pd-U-ace-NH-A. Furthermore, results ^{1}H NMR pattern [Supplementary Figure 11], TG [Supplementary Figure 12], and Pd 3d XPS spectra [Supplementary Figure 13 and Supplementary Table 4] suggested that compared with the fresh Pd-U-ace-NH, the missing linker defects and surface Pd^0 species of Pd-U-ace-NH-A were increased after o-xylene degradation. Therefore, the improvement of the catalytic performance for o-xylene degradation over Pd-U-ace-NH-A was ascribed to the increased surface area, missing linker defects and the surface Pd^0 species.

CONCLUSIONS

In conclusion, residual Cl species in acetic acid-modified Pd-UiO-67 catalysts were removed via silver nitrate precipitation and dilute ammonia washing, and the regulation effects of Cl removal on catalyst structure, Pd active sites, o-xylene catalytic degradation and chlorinated byproduct formation were systematically investigated. Compared with Pd-U-ace, the removal of residual Cl species caused the decrease of catalytic performance for o-xylene degradation, which was ascribed to the reduction of missing linker defects, the aggregation of Pd particles, and the decrease of surface Pd^0 species. Notably, both silver nitrate precipitation and dilute ammonia washing can effectively remove residual Cl species in the UiO-67 framework to reduce the generation of Cl-containing byproducts during VOCs degradation. Meanwhile, Pd-U-ace-NH prepared by dilute ammonia washing almost completely inhibits the generation of 4-chloro-1,2-dimethylbenzene and only produces trace 2-chlorotoluene, showing better byproduct control performance than the silver nitrate precipitation method. Importantly, the Pd-U-ace-NH catalyst has excellent long-term stability, reversible water resistance, and reusability. This work demonstrates that dilute ammonia washing is an effective strategy to remove residual Cl in Pd-UiO-67 and suppress toxic Cl-containing byproducts, which provides a feasible route for green synthesis and practical application of Zr-UiO-based noble metal catalysts in VOCs catalytic oxidation. Meanwhile, benefiting from its stability, water resistance, and superior toxic byproduct suppression capability, the optimized Pd-U-ace-NH catalyst is promising for practical deployment in industrial VOC abatement, such as the purification of aromatic VOCs exhaust from petrochemical, coating and printing processes under humid conditions.

DECLARATIONS

Authors' contributions

Made substantial contributions to conception and design of the study and performed data analysis and interpretation: Bi, F.; Yu, H.; Ma, J.; Wang, H.; Huang, J.; Wei, J.; Du, Q.

Performed data acquisition and provided administrative, technical, and material support: Huang, Y.; Zhang, X.

Availability of data and materials

All data required to support the conclusions of this paper are included in the manuscript and the Supplementary Materials. Additional data related to this paper can be obtained from the corresponding authors upon request.

AI and AI-assisted tools statement

Not applicable.

Financial support and sponsorship

This work was supported by the National Natural Science Foundation of China (No. 22506124 and No. 12175145) and the Shanghai Rising-Star Program (24YF2729800). The authors acknowledge the support of the Energy Science and Technology discipline under the Shanghai Class IV Peak Disciplinary Development Program.

Conflicts of interest

All authors declared that there are no conflicts of interest.

Ethical approval and consent to participate

Not applicable.

Consent for publication

Not applicable

Supplementary Materials

Supplementary Materials

REFERENCES

1. Jia, H.; Yao, S.; Tang, X.; et al. Multi-objective machine learning for health-oriented O_3 and $PM_{2.5}$ control: Integrating VOC photochemical consumption and source apportionment. *J. Hazard. Mater.* **2026**, *505*, 141483. DOI PubMed

2. Sun, R.; You, G.; Song, D.; Feng, M.; Liu, H.; Xie, S. Characteristics and sources of ambient VOCs under varying $PM_{2.5}$ levels in winter. *Atmos. Environ.* **2026**, *370*, 121826. DOI
3. Biard, P. Volatile organic compounds absorption in non-aqueous solvents: a critical review based on hydrodynamics and mass transfer considerations. *Chem. Eng. J.* **2025**, *512*, 162413. DOI
4. Liang, W.; Ma, C.; Zhu, Y.; Liu, J. Performance and mechanism of modified red mud for the toluene adsorption. *J. Environ. Chem. Eng.* **2025**, *13*, 115587. DOI
5. Zhang, S.; Yao, L.; Xu, B.; Yang, L.; Dai, Z.; Jiang, W. Recent advances in zeolite-based materials for volatile organic compounds adsorption. *Sep. Purif. Technol.* **2024**, *350*, 127742. DOI
6. Zhang, Y.; Sun, J.; Pan, W.; et al. CeO_2-based catalysts for photocatalytic degradation of volatile organic compounds: a comprehensive review. *J. Environ. Manage.* **2025**, *389*, 126146. DOI PubMed
7. Liu, Y.; Wang, Z.; Chen, P.; Chen, L.; Yin, S. Universal pseudo-fluctuation engineering induces local free radical surface confinement effect to enhance photocatalytic oxidation of toluene. *Appl. Catal. B:. Environ. Energy.* **2026**, *380*, 125806. DOI
8. Feng, Y.; Chu, P.; Hou, Z.; et al. Single-atom catalysts in the photothermal catalysis: fundamentals, mechanisms, and applications in VOCs oxidation. *Chem. Synth.* **2025**, *5*, 64. DOI
9. Zhong, X.; Fang, H.; Chen, J.; Shen, J.; Rui, Z. Micro-environmental modulation of TiO_2-supported bimetallic CuAg by carbon quantum dots for promoting photothermal catalytic VOCs degradation. *Catal. Sci. Technol.* **2025**, *15*, 6513-23. DOI
10. Chen, X.; Weng, B.; Pan, X.; et al. Unraveling the trade-off effect of oxygen vacancies for photothermal catalytic mineralization of multicomponent VOCs under convergent ambient sunlight. *Appl. Catal. B. Environ. Energy.* **2026**, *380*, 125752. DOI
11. Guo, W.; Hao, Z.; Wang, Q.; et al. Targeted regulation of d-band center in $LaCo_{1-x}Ni_xO_3$ perovskite toward Sabatier-optimized catalytic oxidation of VOCs. *Appl. Catal. B:. Environ. Energy.* **2025**, *378*, 125640. DOI
12. Chen, J.; Fang, Q.; Yu, H.; et al. Oxygen vacancy regulation in Cobalt-based catalysts for the degradation of volatile organic compounds: strategies and mechanisms. *J. Colloid. Interface. Sci.* **2026**, *709*, 139931. DOI PubMed
13. Ben Soltan, W.; Souli, I.; Sboui, M.; et al. Unveiling highly active sites on ZSM-5 zeolite modified with Ti and Mn metals: insights into the catalytic oxidation mechanism of VOCs. *J. Environ. Chem. Eng.* **2026**, *14*, 120551. DOI
14. Li, X.; Lu, X.; Zhou, S.; Yao, C.; Chen, Y. Engineering atomically dispersed Pd on nanomineral supported CeO_2 via photo-deposition for low-temperature catalytic oxidation of VOCs. *Chem. Eng. J.* **2026**, *530*, 173431. DOI
15. Pang, J.; Li, Q.; Su, G.; et al. Tailoring dual high-valence Cu-O-Mn active sites to enhance VOC catalytic oxidation. *Environ. Sci. Technol.* **2025**, *59*, 9812-26. DOI PubMed
16. Tan, Z.; Du, X.; Wang, P.; et al. Engineering oxygen vacancy in metal oxides for catalytic oxidation of VOCs: classification, catalytic effects, and construction strategies. *Coord. Chem. Rev.* **2026**, *560*, 217911. DOI
17. Yang, W.; He, T.; Huang, W.; Zhang, Y.; Shan, W.; An, T. Tunning Pd local environments for catalytic oxidation of light VOCs and CO: influence of Ce addition. *J. Environ. Sci.* **2026**. DOI
18. Li, J.; Xu, Z.; Wang, T.; et al. A versatile route to fabricate Metal/UiO-66 (Metal = Pt, Pd, Ru) with high activity and stability for the catalytic oxidation of various volatile organic compounds. *Chem. Eng. J.* **2022**, *448*, 136900. DOI
19. Xu, Z.; Li, J.; Wang, X.; Wang, T.; Li, D.; Ao, Z. Pt-Co bimetals supported on UiO-66 as efficient and stable catalysts for the catalytic oxidation of various volatile organic compounds. *Mater. Today. Chem.* **2023**, *29*, 101403. DOI
20. Li, J.; Xu, Z.; Zhou, J.; et al. Electron-deficient Pt NPs/UiO-66 catalysts: boosting efficiency and suppressing toxic byproducts in the oxidation of diverse volatile organic compounds. *Appl. Catal. B. Environ. Energy.* **2026**, *390*, 126627. DOI
21. Xie, J.; He, X.; Liu, K.; Li, W.; Li, Z. Carboxylic acid modulated *in situ* growth of Zr-based MOFs on carboxylated cotton fabrics for removal of Cr(VI) from aqueous solutions. *Sep. Purif. Technol.* **2024**, *351*, 128043. DOI
22. Vo, T. K.; Le, V. N.; Quang, D. T.; Song, M.; Kim, D.; Kim, J. Rapid defect engineering of UiO-67 (Zr) via microwave-assisted continuous-flow synthesis: effects of modulator species and concentration on the toluene adsorption. *Micropor. Mesopor. Mater.* **2020**, *306*, 110405. DOI
23. Su, S.; Cao, Y.; Ren, Y.; Jiang, H.; Wu, W. Tuning the electronic states of Pd(II) defect-engineered metal-organic framework catalysts for efficient conversion of isocyanides. *Commun. Chem.* **2025**, *8*, 105. DOI PubMed PMC
24. Bi, F.; Feng, X.; Huang, J.; et al. Unveiling the influence mechanism of impurity gases on Cl-containing byproducts formation during VOC catalytic oxidation. *Environ. Sci. Technol.* **2025**, *59*, 15526-37. DOI PubMed
25. Bi, F.; Wei, J.; Gao, B.; et al. How the most neglected residual species in MOF-based catalysts involved in catalytic reactions to form toxic byproducts. *Environ. Sci. Technol.* **2024**, *58*, 19797-806. DOI PubMed
26. Lu, Z.; Guo, L.; Bi, F.; et al. Insight into the degradation mechanism of mixed VOCs oxidation over Pd/UiO-66(Ce) catalysts: combination of operando spectroscopy and theoretical calculation. *Sep. Purif. Technol.* **2025**, *354*, 129443. DOI

27. Dong, X.; Lin, Y.; Ma, Y.; Zhao, L. Ce-doped UiO-67 nanocrystals with improved adsorption property for removal of organic dyes. *RSC. Adv.* **2019**, *9*, 27674-83. DOI PubMed PMC
28. Zhang, Y.; Liu, H.; Wang, D.; Qu, W.; Tian, Z. Enhancing the catalytic performance of Pt-Sn-TiO_2 catalyst for aqueous-phase water-gas shift reaction by constructing an oxide-covered metal particle structure. *Chem. Eng. J.* **2026**, *535*, 175793. DOI
29. Shan, C.; Jia, Q.; Zhang, Y.; et al. Defect engineering regulating the electronic structure of Pt/TiO_2 to tackle the trade-off between activity and SO_2 resistance during CO catalytic oxidation. *J. Catal.* **2026**, *459*, 116922. DOI
30. Zhai, Y.; Zhang, Y.; Gao, X.; et al. Machine-learning-assisted intelligent identification of antibiotics using a rare-earth-functionalized metal-organic frameworks fluorescent sensor. *Dyes. Pigments.* **2026**, *251*, 113730. DOI
31. Sang, J. L.; Liu, Q.; Zhang, Y.; Liu, M. Interface-assembled batch synthesis of homogeneous 2D-AgPd nanosheets toward electrocatalytic CO_2 to CO. *Greenverse. Sci.* **2026**, *1*, 5. DOI
32. Zhou, D.; Zhang, Z.; Dong, H.; et al. *In situ* electronic modulation of g-C_3N_4/UiO66 composites via N species functionalized ligands for enhanced photocatalytic CO_2 reduction. *Sep. Purif. Technol.* **2025**, *379*, 134964. DOI
33. Guo, X.; Dong, C.; Gao, M.; et al. Crystal-facet-dependent activity and N_2 yield of Ag/CeO_2 catalysts for catalytic oxidation of N, N-Dimethylformamide. *Appl. Catal. B. Environ.* **2024**, *341*, 123286. DOI
34. Lv, S.; Guo, F.; Li, K.; Wang, D.; Gao, H.; Song, C. The synergistic effect of Cl doping and Bi coupling to promote the carrier separation of BiOBr for efficient photocatalytic nitrogen reduction. *J. Colloid. Interface. Sci.* **2025**, *677*, 831-41. DOI PubMed
35. Xu, L.; Wang, J.; Li, Y.; et al. Heterointerfacial charge modulation of p-Type covalent organic frameworks on graphene achieving high-performance Cl^- ion storage with ultralong cycling life. *Angew. Chem. Int. Ed.* **2025**, *64*, e202508092. DOI PubMed
36. Zhang, K.; Dai, L.; Liu, Y.; et al. Insights into the active sites of chlorine-resistant Pt-based bimetallic catalysts for benzene oxidation. *Appl. Catal. B. Environ.* **2020**, *279*, 119372. DOI
37. Dong, F.; Meng, Y.; Ling, W.; et al. Single atomic Pt confined into lattice defect sites for low-temperature catalytic oxidation of VOCs. *Appl. Catal. B. Environ. Energy.* **2024**, *346*, 123779. DOI
38. Zheng, Y.; Xu, W.; Yang, J.; et al. Catalytic oxidation of VOCs and CO on cobalt-based Materials: strategies and mechanisms for improving activity and stability. *Chem. Eng. J.* **2024**, *484*, 149296. DOI
39. Xiang, W.; Zhang, Y.; Chen, Y.; Liu, C.; Tu, X. Synthesis, characterization and application of defective metal-organic frameworks: current status and perspectives. *J. Mater. Chem. A.* **2020**, *8*, 21526-46. DOI